• Basic Research •

IL-17A mediates inflammation-related retinal pigment epithelial cells injury *via* ERK signaling pathway

Hui-Min Zhong[1,2,3,4,5], *Bing-Qiao Shen*[1,2,3,4,5], *Yu-Hong Chen*[1,2,3,4,5], *Xiao-Huan Zhao*[1,2,3,4,5], *Xiao-Xu Huang*[1,2,3,4,5], *Min-Wen Zhou*[1,2,3,4,5], *Xiao-Dong Sun*[1,2,3,4,5]

[1]Department of Ophthalmology, Shanghai General Hospital (Shanghai First People's Hospital), Shanghai Jiao Tong University, School of Medicine, Shanghai 200080, China
[2]National Clinical Research Center for Ophthalmic Diseases, Shanghai 200080, China
[3]National Clinical Research Center for Eye Diseases, Shanghai 200080, China
[4]Shanghai Key Laboratory of Fundus Diseases, Shanghai 200080, China
[5]Shanghai Engineering Center for Visual Science and Photomedicine, Shanghai 200080, China
Co-first authors: Hui-Min Zhong and Bing-Qiao Shen
Correspondence to: Min-Wen Zhou and Xiao-Dong Sun. Department of Ophthalmology, Shanghai General Hospital, School of Medicine, Shanghai Jiao Tong University, 100 Hai Ning Road, Shanghai 200080, China. zmw8008@163.com; xdsun@sjtu.edu.cn
Received: 2024-08-26 Accepted: 2024-11-05

Abstract

● **AIM:** To investigate whether interleukin-17A (IL-17A) gets involved in the mechanisms of inflammation-related retinal pigment epithelium (RPE) cells injury and its significance in age-related macular degeneration (AMD).

● **MRTHODS:** A sodium iodate ($NaIO_3$) mouse model as well as *IL-17A*$^{-/-}$ mice were established. The effects of inflammatory cytokines in RPE cells and retinal microglia before and after $NaIO_3$ modeling *in vivo* and *in vitro*, were investigated using immunofluorescence, immunoprotein blotting, and quantitative real-time fluorescence polymerase chain reaction (qRT-PCR), respectively. Interventions using recombinant IL-17A protein (rIL-17A) or IL-17A neutralizing antibody (IL-17A NAb) were used to observe the subsequent differences in fundus, fundus photography and optical coherence tomography (OCT), cell viability, and expression of oxidative stress-related markers before and after modeling, and to screen for key signaling pathways.

● **RESULTS:** In the scenario of $NaIO_3$ stimulation, RPE cells obviously tended to degenerate. Simultaneously proliferation and activation of retinal microglia was confirmed in $NaIO_3$-stimulated mice, whereas such effects induced by $NaIO_3$ were significantly ameliorated with IL-17A NAb intervention or in *IL-17A*$^{-/-}$ mice. In addition, IL-17A promoted the proliferation and activation of microglia as well as oxidative damage and the secretion of inflammatory cytokines alongside $NaIO_3$-induced damage in RPE cells *in vivo* and *ex vivo*. Meanwhile, the extracellular signal-regulated kinase (ERK) signaling pathway was shown to be participated in the regulation of $NaIO_3$-induced RPE cells injury mediated by IL-17A *in vivo* and *ex vivo*, as IL-17A-induced inflammatory cytokines release in the $NaIO_3$ model was alleviated after blocking the ERK pathway.

● **CONCLUSION:** IL-17A probably promotes the $NaIO_3$-induced RPE cells injury through exacerbating inflammation in terms of retinal microglia activation and inflammatory cytokines release *via* ERK signaling pathway. Inhibition of IL-17A may be a new potential target for dry AMD treatment.

● **KEYWORDS:** age-related macular degeneration; retinal pigment epithelium; $NaIO_3$; microglia; IL-17A
DOI:10.18240/ijo.2025.01.03

Citation: Zhong HM, Shen BQ, Chen YH, Zhao XH, Huang XX, Zhou MW, Sun XD. IL-17A mediates inflammation-related retinal pigment epithelial cells injury *via* ERK signaling pathway. *Int J Ophthalmol* 2025;18(1):15-27

INTRODUCTION

Age-related macular degeneration (AMD) is the leading cause of incurable blindness in people over the age of 55y[1]. The etiology of dry AMD remains unclear, and the final pathological manifestation of advanced dry AMD is geographic atrophy (GA), which is currently incurable. One of the pathological characteristics of GA is prominent inflammation, with activated microglia and macrophages abundantly present in the degenerative area[2-3]. Increasing evidence suggests that oxidative stress and immune inflammation perform critical roles in the occurrence and development of GA. As a key part of the blood-retinal barrier, retinal pigment epithelium (RPE) is sensitive to excessive oxidative stress[4-5]. Additionally, RPE is strongly associated with immunoinflammatory

mechanisms in the posterior segment of the eye. It has been reported that damaged RPE triggers the secretion of a series of inflammatory cytokines and chemokines. As aging progresses, damage caused by oxidative stress gradually accumulates, leading to inflammation through various pathways, which can result in the death of local retinal cells and ultimately form GA lesions[6-7].

Among the interleukin (IL)-17 family, IL-17A is most closely related to human health and disease, playing crucial roles in immune-inflammatory responses, angiogenesis, and barrier integrity[8-9]. IL-17A is also involved in the pathogenesis of various eye diseases such as AMD, diabetic retinopathy, autoimmune uveitis, and glaucoma[10-12]. We have previously systematically reviewed the IL-17 signaling pathway in relation to the development of AMD[13]. The study demonstrated that serum levels of IL-17 were significantly lower in normal subjects than in patients with AMD, mainly in both neovascular and geographic atrophic types of AMD[14-16]. It has been shown that the IL-17 signaling pathway was involved in the inflammatory response to oxidative stress modulated by 4-octyl itaconate in human RPE cells[17]. Additionally, enrichment analysis revealed that the upregulated genes in RPE samples from AMD patients were mainly involved in the IL-17 signaling pathway[18]. Chronic neuroinflammation is one of the causes of dry AMD, with retinal microglia being the resident primary cells took part in the immune-inflammatory responses in both optic nerve and retina. Microglia plays a crucial role in initiating and sustaining inflammatory responses, as in central neurodegenerative diseases, most literature suggests that IL-17A primarily activates microglia, leading to disease onset and progression[19-22].

In summary, both IL-17A and retinal microglia engage in the inflammatory process of dry AMD. However, the relationship between RPE cells injury, IL-17A, retinal microglia activation and inflammatory factors release in the occurrence and development of AMD have not been fully elucidated. It is necessary to clarify the interactions within the above meshwork, investigate their roles and relationships in AMD, and identify the related signaling pathways, which will help identify new therapeutic targets and enrich the understanding of AMD pathogenesis.

MATERIALS AND METHODS

Ethical Approval The experiments of animals in this study were approved by the Ethics Committee of Shanghai general Hospital Shanghai Jiao Tong University School of Medicine (Approval number: 2023AWS304), China and complied with the guidelines of the Association for Research in Vision and Ophthalmology for the use of animals in vision and ophthalmic research. Furthermore, all experimental procedures involving animals were conducted under local or general anesthesia in accordance with ethical principles for animal welfare protection.

Cell Culture and Treatment Adult retinal pigment epithelial cell (ARPE)-19 cells were cultured in Dulbecco's Modified Eagle Medium F-12 (DMEM-F12; 1:1, Gibco, USA) containing 10% fetal bovine serum (FBS; Gibco, USA). After selecting the appropriate intervention concentration, we induced damage with sodium iodate ($NaIO_3$) at different time points (0, 2, 4, 8, 12, 24h). Subsequently, the cells were pretreated with recombinant IL-17A protein (rIL-17A, 100 ng/mL) and IL-17A neutralizing antibody (IL-17A NAb, 100 ng/mL) for 24h, followed by $NaIO_3$-induced damage, and then relevant assays were performed to assess the indicators.

Animals This study utilized specific pathogen-free grade adult male C57BL/6 mice and *IL-17*$^{-/-}$ mice (6-8wk, 18-25 g), provided by the Experimental Animal Center of Shanghai Jiao Tong University Affiliated Shanghai General Hospital. All mice were housed in accordance with the Regulations on the Management of Laboratory Animals in the animal facility of the Shanghai General Hospital. The housing environment was maintained at a 12-hour light/dark cycle and a temperature of 22℃-26℃ with 60% humidity. Before the experiment, all mice underwent a comprehensive ophthalmic examination, and those not meeting the experimental criteria were excluded.

$NaIO_3$ Mouse Model A 1% $NaIO_3$ stock solution was prepared by dissolving $NaIO_3$ powder in sterile saline or phosphate-buffered saline (PBS). The mice were then intraperitoneally injected with $NaIO_3$ at a dose of 40 mg/kg. Tissue samples were collected at 3, 5 and 7d post-injection.

Drug Administration The anesthetic dose was calculated based on the animal's body weight before surgery. After the mice were anesthetized, the dilation of the pupils was confirmed under a surgical microscope. Using a 33G needle microinjector (Hamilton Bonaduz AG, Switzerland), 2 μL of the substance to be injected was drawn up. The needle was inserted into the eye perpendicular to the sclera surface 2 mm behind the temporal limbus, avoiding blood vessels. When a breakthrough sensation was felt, the needle was observed under the microscope to have entered the vitreous cavity, and the insertion was stopped. Then, 2 μL of liquid was injected into the vitreous cavity and slowly withdrawn after maintaining the needle position for 5-10s. After the injection, 0.3% ofloxacin eye ointment was applied to prevent infection.

For the extracellular signal-regulated kinase 1/2 (ERK1/2) pathway inhibitor (PD98059, 10 mg/kg), the solution was prepared by dissolving the powder in dimethyl sulfoxide (DMSO) to make a 4% stock solution, which was then mixed with 30% PEG300, 5% Tween80, and 61% H_2O under sterile conditions in a laminar flow hood, and aliquoted for intraperitoneal injection. Three days before the $NaIO_3$

modeling, the mice were pre-treated with intravitreal injections of rIL-17A (0.5 mg/mL) or IL-17A NAb (0.5 mg/mL) and intraperitoneal injections of PD98059 (10 mg/kg).

Fundus Photography and Optical Coherence Tomography Fundus evaluation of mice was performed using the Phoenix MICRON IV system (Cold Spring Harbor Corp., USA). Guided by real-time imaging, OCT images centered on the optic disc covering the entire retina were obtained, along with 50° field posterior fundus images.

Hematoxylin and Eosin Staining of Mouse Eyes Eyeballs collected from mice were fixed in eyeball fixative overnight. The tissue samples were dehydrated in gradient with ethanol solutions of different concentrations, and then were washed with xylene. The tissues were embedded in paraffin at a specific temperature and prepared for sections. When ready for staining, the sections were rehydrated in ethanol, and then were stained with hematoxylin and eosin (H&E). At last, the sections were placed on a coverslip and prepared for imaging.

Western Blot Proteins of retina tissues and cells were isolated, and their concentrations were measured. These proteins were separated using 12.5% gradient SDS-PAGE (Invitrogen, Carlsbad, CA, USA) and incubated overnight at 4°C with different primary antibodies. The primary antibodies used were listed as follows: mouse anti-β-actin (3700, 1:1000; Cell Signaling Technology), rabbit anti-IL-1β (ab234437, 1:1000; Abcam), rabbit anti-IL-6 (ab233706, 1:1000; Abcam), rabbit anti-tumor necrosis factor-alpha (TNF-α; 3707, 1:1000; Cell Signaling Technology), rabbit anti-ionized calcium-binding adaptor molecule-1 (IBA-1; ab178846, 1:1000; Abcam), rabbit anti-IL-17A (ab79056, 1:1000; Abcam), rabbit anti-TXNIP (ab188865, 1:1000, Abcam), rabbit anti-Occludin (A2601, 1:1000, abclonal), rabbit anti-CD68 (ab201340, 1:200; Abcam), rabbit anti-p38 (8690, 1:1000; Cell Signaling Technology, Boston, MA, USA), rabbit anti-p-p38 (4511, 1:1000; Cell Signaling Technology), rabbit anti-NF-κB (8242, 1:1000; Cell Signaling Technology), rabbit anti-p-NF-κB (3033,1:1000, Cell Signaling Technology), rabbit anti-ERK1/2 (8544, 1:1000; Cell Signaling Technology) and rabbit anti-p-ERK1/2 (4370, 1:1000; Cell Signaling Technology). After rinsed in TBST three times for 10min, the blots were incubated at room temperature with HRP-conjugated secondary antibodies (Jackson ImmunoResearch Laboratories, West Grove, PA, USA) for 90min. Densitometry was detected by the enhanced chemiluminescence detection reagents (ImageQuant LAS4000) and then analyzed by Image J software.

Quantitative RT-PCR Analysis Total RNA was extracted from mouse retina or cells using TRIzol® reagent according to the manufacturer's protocol (InvitrogenTM, Waltham, MA, USA). The RNA quality was determined using a NanoDrop instrument (Thermo Fisher Scientific, Waltham, MA, USA). The optical density (OD) value ratio of 260 nm/280 nm was tested for the sample (1 μL) to calculate the RNA concentration, using diethyl pyrocarbonate water (Sangon Biotech, Shanghai, China) as the control. RNA was reverse transcribed into cDNA using the PrimeScript™ RT Master Mix (Takara, Tokyo, Japan) transcriptase kit. The RNA volume needed for reverse transcription was calculated based on the RNA concentration (20 μL volume containing 2000 ng RNA), and the RNA volume was mixed with 4 μL PrimeScript RT Master Mix and RNase Free dH_2O was added to make up a total volume of 20 μL. Quantitative real-time PCR was performed using the TB Green™ Premix Ex Taq™ (Takara Bio, Inc., Japan) on a 7500 real-time PCR system (Applied Biosystems, Foster City, CA, USA) with a total volume of 20 μL. The primer pairs used are as follows: *GAPDH* (F: CAGGAGGCATTGCTGATGAT, R: GAAGGCTGGGGCTCATTT); *IL-1β* (F: GGACAGGATATGGAGCAACAAGTGG, R: TCATCTTTCAACACGCAGGACAGG); *IL-6* (F: GACAGCCACTCACCTCTTCAGAAC, R: GCCTCTTTGCTGCTTTCACACATG); *TNF-α* (F: AGCCCTGGTATGAGCCCATCTATC, R: TCCCAAAGTAGACCTGCCCAGAC).

Immunofluorescence Analysis for Retinal Whole Mounts On the 3rd, 5th, and 7th days after $NaIO_3$-induced RPE damage *in vivo*, retinal tissue was collected and flat-mounted. Mice were fully anesthetized before perfusion. Once the limbs of the mice stiffened, the eyeballs were immediately enucleated and fixed in 4% paraformaldehyde at 4°C for 1h, then isolating the retina. The retinas were permeabilized with 0.3% Triton X-100 at room temperature for 30min, then blocked with 5% bovine serum albumin (Sigma-Aldrich) for 1h to remove nonspecific staining. Rabbit monoclonal anti-IBA-1 (Abcam, catalog number ab178846, dilution 1:200) and rabbit anti-mouse zonula occludens protein 1 (ZO-1) polyclonal antibody (Invitrogen, catalog number 40-2200, dilution 1:50) were added and incubated overnight at 4°C. The following day, the retinas were incubated with Alexa Fluor® 555-conjugated donkey anti-rabbit secondary antibody (Invitrogen, catalog number A31572, dilution 1:500) in the dark at 37°C for 1-2h. The retinas were then mounted on slides with the inner surface facing up, cut into a clover shape, and covered with fluorescence mounting medium (DAKO, catalog number S3023) and a coverslip. Fluorescence images were observed using a laser scanning confocal microscope (LSM 510 META; Zeiss, Jena, Germany).

Immunofluorescence Analysis for Retinal Cryosection The required eyeballs were fixed overnight with 4% paraformaldehyde. After gradient dehydration in different sucrose concentrations, the eyeballs were embedded in optimum cutting temperature compound and frozen at -20°C.

The tissues were sectioned into 10 μm thick slices using a Leica CM1950 cryostat (Leica, Wetzlar, Germany). The sections were permeabilized and blocked for 1h. Rabbit monoclonal anti-IBA-1 antibody was added, and incubated overnight at 4°C. The fluorescent secondary antibody was performed in a humidified chamber at 37°C for 1h, kept away from light. The nuclei were marked by 4',6-diamidino-2-phenylindole. Images were obtained using a Zeiss LSM 980 confocal fluorescence microscope.

Immunofluorescence Analysis for ARPE-19 RPE cells were seeded at 1×10^5 cells/well in a 24-well plate with pre-placed cell climbing slides. The adhered cells were treated with rIL-17A and IL-17A NAb. The cells were washed sufficiently with PBS, fixed for 15min, incubated for 20min, followed by blocking for 1h. Rabbit anti-mouse ZO-1 polyclonal antibody was added, and the cells were incubated overnight at 4°C. The fluorescent secondary antibody was performed in a humidified chamber at 37°C for 1h, kept away from light. The cells were washed three times with PBS, 10min each time, and the cell climbing slides were inverted onto microscope slides pre-dropped with fluorescence mounting medium (with the cell side facing down). The images were captured using a confocal microscope.

Reactive Oxygen Species Detection The detection of intracellular reactive oxygen species (ROS) was conducted using the fluorescent probe 2',7'-dichlorodihydrofluorescein diacetate (DCFH-DA; Beyotime, China). RPE cells were first stimulated with drugs, specifically rIL-17A and IL-17A NAb, before loading the probe. After drug stimulation, the diluted DCFH-DA (1:1000, 10 μmol/L) was added to adequately cover the cells, incubating at 37°C for 20min. Following incubation, the cells were washed fully with serum-free culture medium for 10min each time to thoroughly remove any extracellular DCFH-DA. Observation was then conducted using a laser microscope with an emission wavelength of 525 nm and an excitation wavelength of 488 nm.

Nitric Oxide Detection The nitric oxide assay kit (NO, Beyotime, China) was primarily used to detect the nitric oxide content in the supernatant of cell cultures. Standards and collected supernatants from cells treated with $NaIO_3$, rIL-17A or IL-17A NAb were added to a 96-well plate at 50 μL/well. Griess Reagent I and Griess Reagent II were subsequently added to each well. The absorbance was measured using a microplate reader at a wavelength of 540 nm, and the NO content was calculated.

Cell Counting Kit Assay RPE cells survivability was tested by using cell counting kit-8 (CCK-8) assay (Yeason, China). RPE cells were counted and inoculated in 96-well plates with an inoculum volume of not less than 2500 cells/well. Briefly, after different treatments (0, 2, 4, 5, 8, 10, and 15mmol/L) of $NaIO_3$ for 24h, 10 μL of CCK-8 were put into a 96-well plate and incubated at 37°C for maximum 4h. The OD value at 450 nm was measured by a microplate photometer.

Statistical Analysis Data analyses were performed with Image J software (National Institutes of Health, Bethesda, MD, USA), GraphPad prism9.0 (GraphPad Software, Inc., La Jolla, CA, USA) and SPSS 18.0 software (IBM, Corp., Armonk, NY, USA). First, the Kolmogorov-Smirnov test was used to check for normality. For comparisons involving multiple groups, one-way ANOVA was used for pairwise comparisons between groups. All data were presented as mean±standard deviation (SD), and a $P<0.05$ was considered statistically significant.

RESULTS

Establishment of $NaIO_3$-induced RPE Cells Injury Model *in Vitro* and *in Vivo* Fundus photography and OCT images were taken of mice modelled on days 0, 3, 5, and 7 after intraperitoneal injection of $NaIO_3$ (40 mg/kg). The results showed that $NaIO_3$-induced retinal degeneration progressively worsened as the time extended after modelling. Typical phenotypic changes were already present from day 3. The detachment of RPE flakes on day 5 and day 7 progressively worsened. On day 7 there was already a complete structural disorganisation and the inner and outer segments of the photoreceptors did not exist (Figure 1A). On the other hand, H&E staining showed that $NaIO_3$ caused loss of RPE integrity and aggregation of melanin granules, with significant thinning of outer nuclear layer (ONL; Figure 1B). To investigate the relationship between the expression of the barrier-related protein Occludin and the oxidative stress-related protein TXNIP in RPE cells following $NaIO_3$ induction and RPE damage, Western blot analysis was performed on retina from mice treated with intraperitoneal injection of $NaIO_3$ (40 mg/kg) at 0, 3, 5, and 7d. The results showed that with increasing induction duration, the expression of Occludin progressively and significantly decreased (Figure 1D; $P<0.05$), indicating progressive barrier disruption of RPE cells connections. In contrast, the expression trend of the oxidative stress-related protein TXNIP was completely opposite as it gradually increased with prolonged induction duration (Figure 1D; $P<0.05$). These data suggested that $NaIO_3$ stimulation led to a decrease in the expression of the barrier protein Occludin in mouse RPE, exacerbating oxidative stress responses.

To determine the optimal concentration of $NaIO_3$ for stimulating RPE cells *in vitro*, RPE cells were treated with varying concentrations of $NaIO_3$. The results of the CCK-8 assay indicated that as the concentration of $NaIO_3$ increased, the number of ARPE-19 cells gradually decreased and cell viability progressively declined, with almost no cell survival at a concentration of 15 mmol/L. Due to its concentration-dependent effects, a concentration of 5 mmol/L, which maintains over 90% cell viability, was selected as the optimal

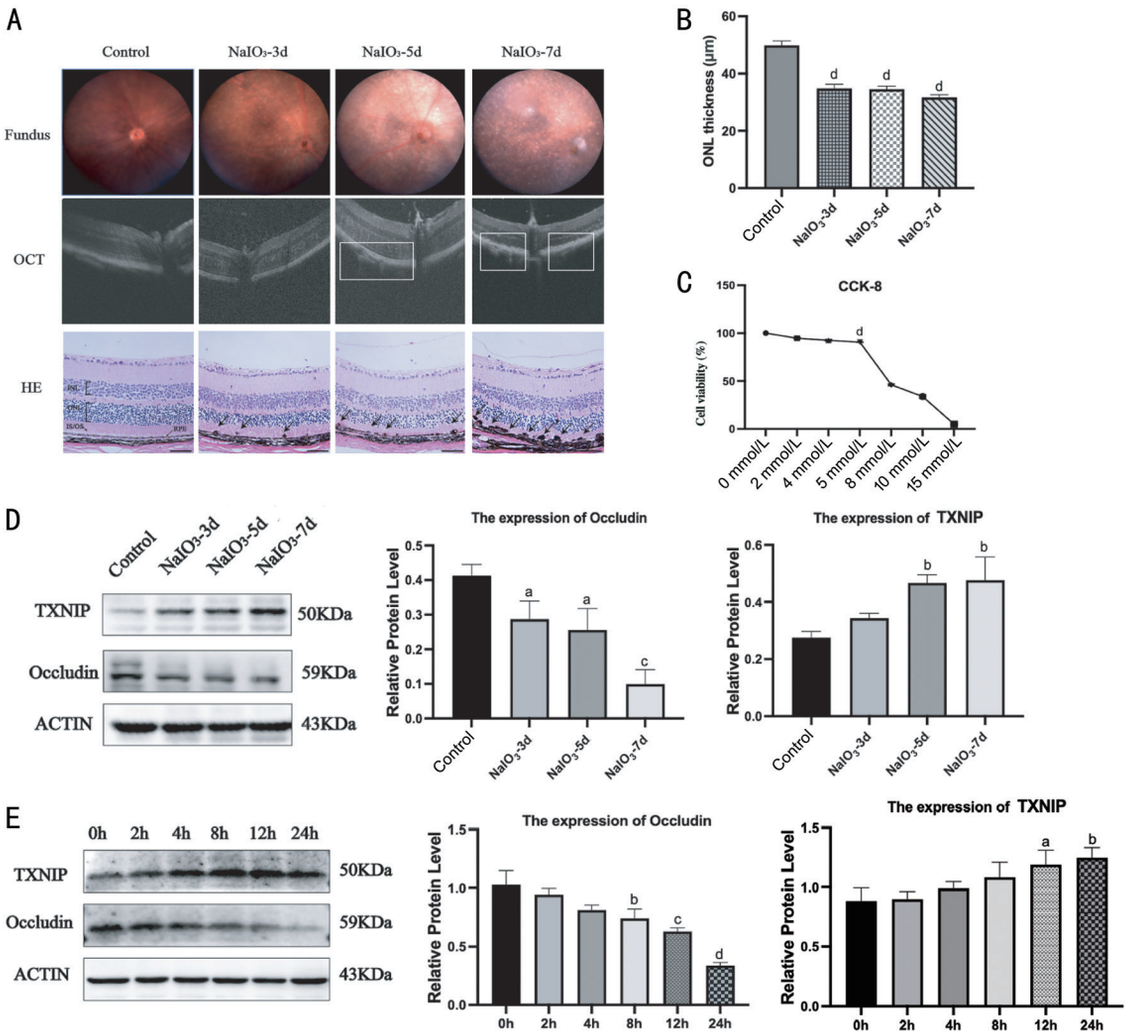

Figure 1 Establishment of $NaIO_3$-induced RPE damage model *in vitro* and *in vivo* A: Fundus images, OCT, and HE staining images obtained from wild-type mice before intraperitoneal injection of $NaIO_3$ (40 mg/kg) and 3, 5, and 7d after injection. Arrows indicate the areas of damage post-injection; Scale bar=50 μm. B: Quantitative data of ONL thickness. C: Percentage of ARPE-19 cell viability following stimulation with different concentrations of $NaIO_3$ (0, 2, 4, 5, 8, 10, 15 mmol/L) was assessed using the CCK-8 assay (n=3/group). D: Western blot analysis and grayscale quantification of Occludin and TXNIP in RPE cells before intraperitoneal injection of $NaIO_3$ (40 mg/kg) and at 3, 5, and 7d after injection (n=3). E: Western blot analysis and grayscale quantification of Occludin and TXNIP in ARPE-19 cells following $NaIO_3$ stimulation at 0, 2, 4, 8, 12, and 24h (n=3). Data were represented as mean±SD, ^aP<0.05, ^bP<0.01, ^cP<0.001, and ^dP<0.0001 *vs* control group. $NaIO_3$: Sodium iodate; INL: Inner nuclear layer; ONL: Outer nuclear layer; IS/OS: Inner/outer segments of the photoreceptors; RPE: Retinal pigment epithelium; OCT: Optical coherence tomography; HE: Hematoxylin and Eosin staining; ARPE-19: Adult retinal pigment epithelial cell-19; CCK-8: Cell counting kit-8.

concentration (Figure 1C). ARPE-19 cells were treated with the optimal concentration of $NaIO_3$ (5 mmol/L) for 0, 2, 4, 8, 12, and 24h. Western blot analysis was then performed. The results showed that with increasing stimulation duration, Occludin expression progressively decreased (Figure 1E; P<0.05), indicating progressive barrier disruption. In contrast, the expression trend of the oxidative stress-related protein TXNIP was completely opposite as it gradually increased with prolonged stimulation (Figure 1E; P<0.05). These findings were consistent with the observations *in vivo*.

IL-17A and Related Pro-inflammatory Cytokines Release and Microglial Activation in $NaIO_3$ Injury Model To investigate the expression of related inflammatory factors in the $NaIO_3$-induced RPE damage model, RPE damage was induced in mice using $NaIO_3$ (40 mg/kg), and the expression of inflammatory factors in retina was observed at 0, 3, 5, and 7d in the *in vivo* damage model. Western blot results showed that the expression of IL-17A, TNF-α, and IL-6 gradually increased, peaking on day 5 and then decreasing on day 7. The expression of IL-1β peaked on day 3 and then gradually decreased (P<0.05; Figure 2A).

RPE cells were stimulated with $NaIO_3$ at a concentration of 5 mmol/L *in vitro*. The expression of IL-17A in ARPE-19 cells was detected at 0, 2, 4, 8, 12, and 24h after stimulation. Western blot results showed that the expression level of IL-17A gradually increased after $NaIO_3$ stimulation, peaking

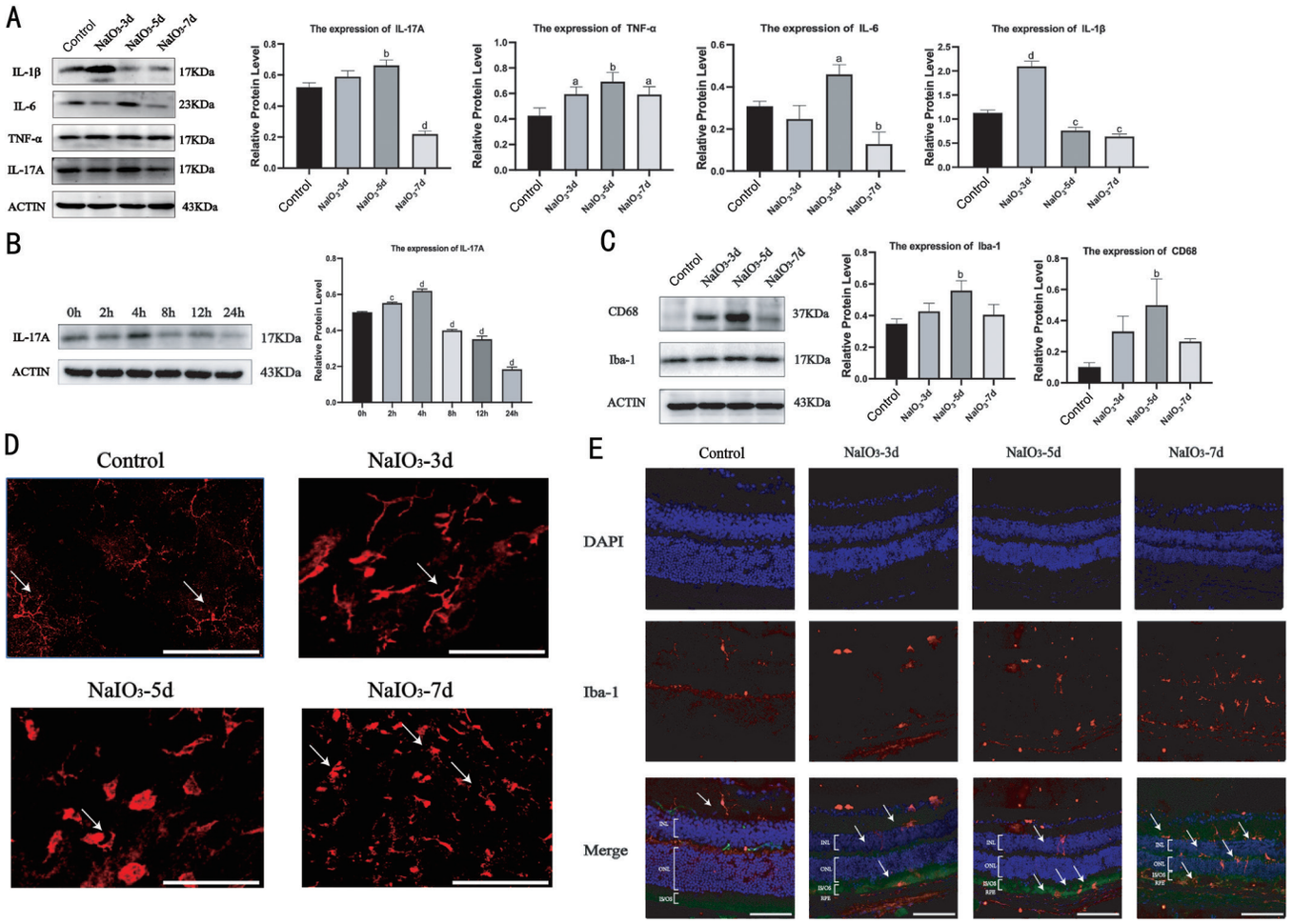

Figure 2 IL-17A and related pro-inflammatory cytokine release and microglial activation in $NaIO_3$ injury model A: Western blot analysis and grayscale quantification of IL-17A, TNF-α, IL-1β, and IL-6 in retina after $NaIO_3$ treatment (n=3). B: Western blot analysis and grayscale quantification of IL-17A in ARPE-19 cells following $NaIO_3$ stimulation at 0, 2, 4, 8, 12, and 24h (n=3). C: Western blot analysis and grayscale quantification of microglial proliferation and activation markers IBA-1 and CD68 in the retinas of control mice and mice at 3, 5, and 7d after $NaIO_3$ modeling (n=3). D: IBA-1 immunofluorescence staining of retinal flat mounts at different time points following $NaIO_3$-induced RPE damage. White arrows indicate microglia. Magnification 200×, scale bar=50 μm. E: IBA-1 immunofluorescence staining of retinal sections at different time points following $NaIO_3$-induced RPE damage (magnification 200×, scale bar=50 μm); Data were represented as mean±SD, ^aP<0.05, ^bP<0.01, ^cP<0.001, and ^dP<0.0001 *vs* control group; $NaIO_3$: Sodium iodate; INL: Inner nuclear layer; ONL: Outer nuclear layer; IS/OS: Inner/outer segments of the photoreceptors; RPE: Retinal pigment epithelium; IBA-1: Ionized calcium-binding adaptor molecule-1; ARPE-19: Adult retinal pigment epithelial cell-19.

at 4h and then slowly decreasing (Figure 2B; P<0.05). These data indicated that the expression of IL-17A is upregulated in ARPE-19 cells under $NaIO_3$ stimulation, with the highest production of IL-17A observed at 4h after stimulation.

Next, we evaluated the role of microglia, which were recognized as the primary initiator and indicator for inflammation in retina, in the $NaIO_3$ model. Western blot analysis, retinal flat mount, and retinal section immunofluorescence staining were performed on retinal tissues of mice 3, 5, and 7d after $NaIO_3$-induced RPE damage. Western blot results showed that compared with the control group, the expression of CD68 and IBA-1 proteins gradually increased in the retina of $NaIO_3$ model mice, peaking on day 5 and then slightly decreasing (Figure 2C; P<0.05).

Retinal flat mount results showed that the number of retinal microglia significantly increased after modeling, and the morphology of microglia changed from a branched resting state to an amoeboid or round activated state (Figure 2D). Retinal section IBA-1 immunofluorescence staining showed that the number of retinal microglia significantly increased after modeling, and the microglia gradually migrated toward ONL, eventually reaching the IS/OS and RPE layers. The morphology of microglia changed from a branched resting state to an amoeboid or round activated state (Figure 2E). In the control group, microglia were only present in the inner plexiform layer (IPL); after $NaIO_3$ stimulation, the IBA-1 positive microglia were observed in the INL, ONL, IS/OS and RPE layer (Figure 2E).

These results suggested that the $NaIO_3$ RPE damage model could lead to proliferation and activation of retinal microglia, which gradually migrated to the outer layers of the retina to exert their effects.

IL-17A Promoted the Release of Pro-inflammatory Factors Associated with RPE Damage and the Activation of Retinal Microglia in $NaIO_3$ Injury Model To verify the impact of IL-17A on the fundus phenotype during $NaIO_3$-induced RPE damage, rIL-17A and IL-17A NAb were intravitreally injected into mice 3d before $NaIO_3$ modeling as a pre-intervention. Fundus photography and OCT imaging were performed on each group of mice on the 5th day after $NaIO_3$ modeling. Compared with the $NaIO_3$ group, the rIL-17A treatment group showed significantly increased sheet-like RPE detachment. However, the IL-17A NAb treatment group showed alleviated RPE damage. OCT images showed that the retinal layers in the control group were flat and smooth, while clear wrinkles and damage appeared after $NaIO_3$ modeling. The rIL-17A treatment group exhibited loss of RPE integrity and increased aggregation of pigment granules, whereas the IL-17A NAb treatment group had significantly reduced RPE damage (Figure 3A).

ARPE-19 cells were treated with or without rIL-17A or IL-17A NAb for 24h following $NaIO_3$ stimulation, and ROS production was quantified using DCFH-DA fluorescent probes. The results showed that $NaIO_3$ stimulation led to increased ROS production in RPE; the $NaIO_3$+rIL-17A treatment group had significantly increased green fluorescence compared to the $NaIO_3$-only group (P<0.05), approximately 2.6 times that of the $NaIO_3$-only group; whereas the $NaIO_3$+IL-17A NAb treatment group had significantly reduced green fluorescence compared to the $NaIO_3$-only group (P<0.05; Figure 3B). Nitric oxide (NO) levels in the culture supernatant were measured, and it was found that NO levels in the $NaIO_3$+rIL-17A treatment group were reduced by 22.4% compared to the $NaIO_3$-only group (n=4, P<0.05), while NO levels in the $NaIO_3$+IL-17A NAb treatment group increased by 36% (n=4, P<0.05; Figure 3C). The results indicated that inhibiting IL-17A can reduce $NaIO_3$-induced oxidative stress in RPE.

Next, we investigated the regulatory role of IL-17A on retinal microglia activation during $NaIO_3$-induced RPE damage by performing Western blot analysis on retinal tissues from the $NaIO_3$ model with or without rIL-17A or IL-17A NAb intervention. The results showed that compared with the $NaIO_3$-only group, the expression of microglial proliferation and activation markers IBA-1 and CD68 in the retina of rIL-17A treatment group significantly increased (P<0.05), while their expression in the IL-17A NAb treatment group obviously decreased (P<0.05; Figure 3D). This indicated that inhibiting IL-17A can reduce microglial proliferation and activation in $NaIO_3$-induced RPE injury model.

To investigate the regulatory role of IL-17A on the expression of inflammatory factors and the barrier-associated protein Occludin in RPE during $NaIO_3$-induced RPE damage, Western blot and RT-PCR analyses were performed on $NaIO_3$-induced RPE damage models *in vivo* and *in vitro*. The results showed that both *in vivo* and *in vitro* models, compared with the $NaIO_3$-only group, the expression of TNF-α, IL-1β, and IL-6 of the rIL-17A treatment group significantly increased (P<0.05), while the expression of Occludin significantly decreased (P<0.05). The IL-17A NAb treatment group exhibited the opposite trend (Figure 3E, 3F).

To better elucidate the morphological impact of IL-17A in $NaIO_3$-induced RPE damage models *in vivo* and *in vitro*, flat mounts and immunofluorescence staining of the RPE-choroid-sclera complex in mice and ARPE-19 cells were performed. The barrier-associated tight junction protein ZO-1 exhibited a hexagonal morphology in the control group; after $NaIO_3$ stimulation, significant morphological changes occurred in RPE both *in vivo* and *in vitro*: cell bodies enlarged, and the number of RPE with characteristic hexagonal morphology decreased. The rIL-17A treatment group showed more disorganized distribution and abnormal morphology of RPE, while the IL-17A NAb treatment group showed some improvement in the distribution and morphology of RPE (Figure 3G).

IL-17A Regulated Proinflammatory Cytokines Release *via* the ERK Signaling Pathway in $NaIO_3$ Model We further investigated the mechanism by which IL-17A may regulate $NaIO_3$-induced RPE damage. Guided by a rigorous literature review, we identified several signaling pathways, including the p38 MAPK signaling pathway, ERK1/2 signaling pathway, and NF-κB signaling pathway. Relevant signaling pathways were screened using ARPE-19 cells *in vitro*. When cells were treated with $NaIO_3$, $NaIO_3$+rIL-17A, or $NaIO_3$+IL-17A NAb, Western blot results showed significant differences in the expression of phosphorylated ERK (p-ERK) protein among these treatments (P<0.05). Specifically, p-ERK expression increased following $NaIO_3$ stimulation alone, and was further elevated with $NaIO_3$+rIL-17A treatment, and oppositely decreased with $NaIO_3$+IL-17A NAb treatment (Figure 4A). By using rIL-17A and the signaling pathway inhibitor PD98059 to intervene in the $NaIO_3$-induced model, we validated the relationship between the ERK signaling pathway and IL-17A in RPE damage. Compared with the $NaIO_3$+rIL-17A treatment group, the expression of related inflammatory factors (IL-1β, TNF-α and IL-6) significantly decreased in the $NaIO_3$+rIL-17A+PD98059 treatment group (P<0.05; Figure 4B). Additionally, intravitreal injection of IL-17A NAb in $NaIO_3$-stimulated mice was used to evaluate p-ERK expression in

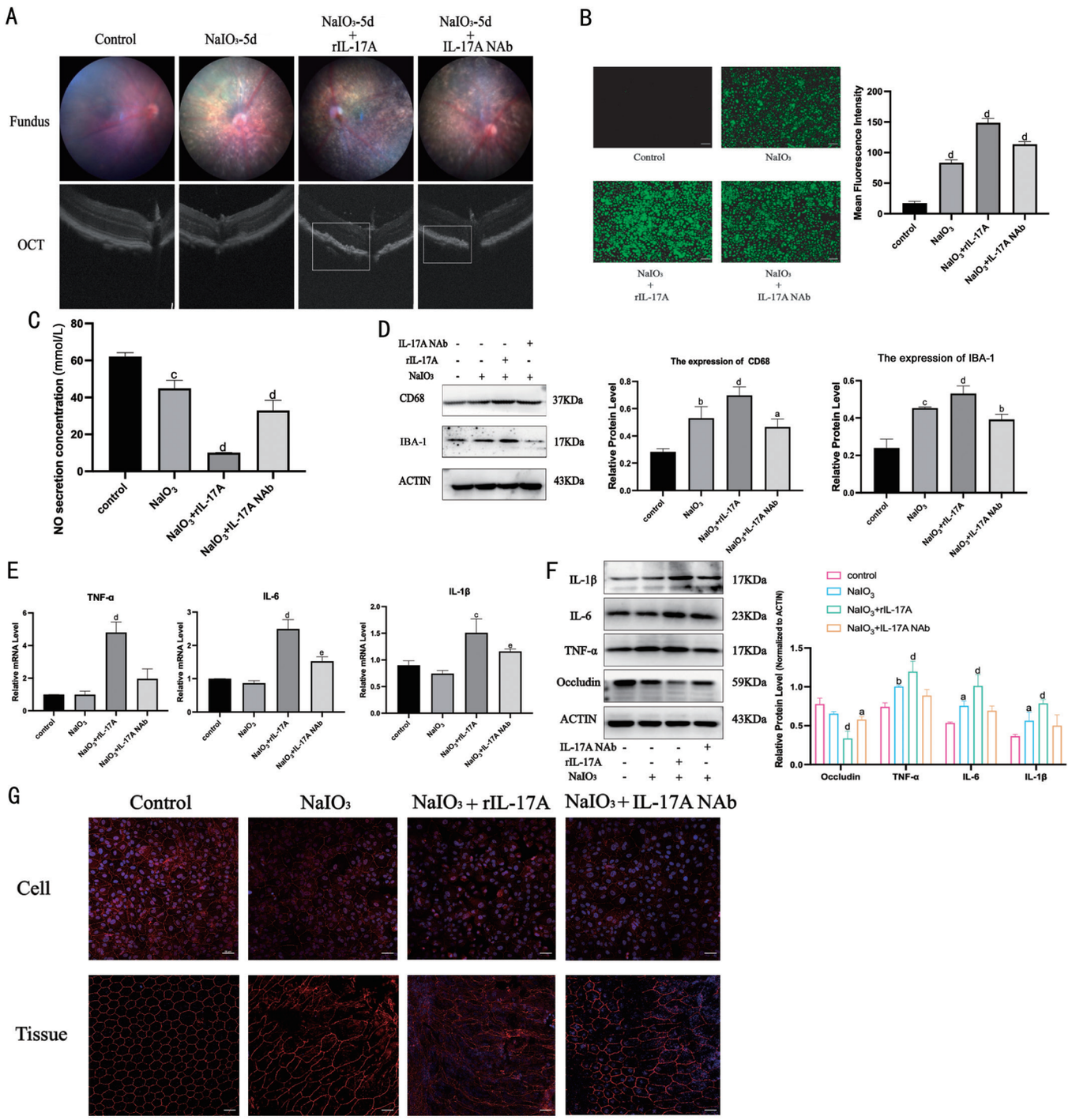

Figure 3 IL-17A promoted the release of pro-inflammatory factors and activation of retinal microglia in $NaIO_3$ RPE damage models A: Fundus and OCT images obtained from wild-type mice pretreated with PBS, rIL-17A, or IL-17A NAb followed by $NaIO_3$ stimulation and the control; B: ARPE-19 cells were pretreated with PBS, rIL-17A or IL-17A NAb for 24h followed by $NaIO_3$ stimulation along with the control. The production of ROS was quantified using a ROS detection kit and the average immunofluorescence intensity was calculated and compared (n=3, magnification 200×, scale bar=50 μm); C: ARPE-19 cells were pretreated with PBS, rIL-17A or IL-17A NAb for 4h followed by $NaIO_3$ stimulation along with the control. The cell culture supernatant was quantitatively analyzed using a NO assay kit. Data are presented as mean±SD. D: The expression changes of IL-17A on the proliferation and activation markers IBA-1 and CD68 of retinal microglia in mice with $NaIO_3$-induced RPE injury (n=3). E: mRNA expression of *TNF-α*, *IL-1β*, and *IL-6* in ARPE-19 cells following $NaIO_3$-induced treatment, with or without intervention by rIL-17A or IL-17A NAb (n=3); F: Western blot analysis and grayscale quantification of TNF-α, IL-1β, IL-6, and Occludin expression in mouse retina following $NaIO_3$-induced damage, with or without intervention by rIL-17A or IL-17A NAb. G: Immunofluorescence staining of barrier-associated tight junction protein ZO-1 *in vivo* and *in vitro* RPE damage models induced by $NaIO_3$, with or without intervention by rIL-17A or IL-17A NAb (magnification 200×, scale bar=50 μm); Data were represented as mean±SD, ^aP<0.05, ^bP<0.01, ^cP<0.001, and ^dP<0.0001 *vs* control group; ^eP<0.05 *vs* $NaIO_3$ group. $NaIO_3$: Sodium iodate; rIL-17A: Recombinant IL-17A protein; IL-17A NAb: IL-17A neutralizing antibody; RPE: Retinal pigment epithelium; OCT: Optical coherence tomography; ARPE-19: Adult retinal pigment epithelial cell-19; PBS: Phosphate-buffered saline; ROS: Reactive oxygen species; IBA-1: Ionized calcium-binding adaptor molecule-1; IL: Interleukin; TNF: Tumor necrosis factor.

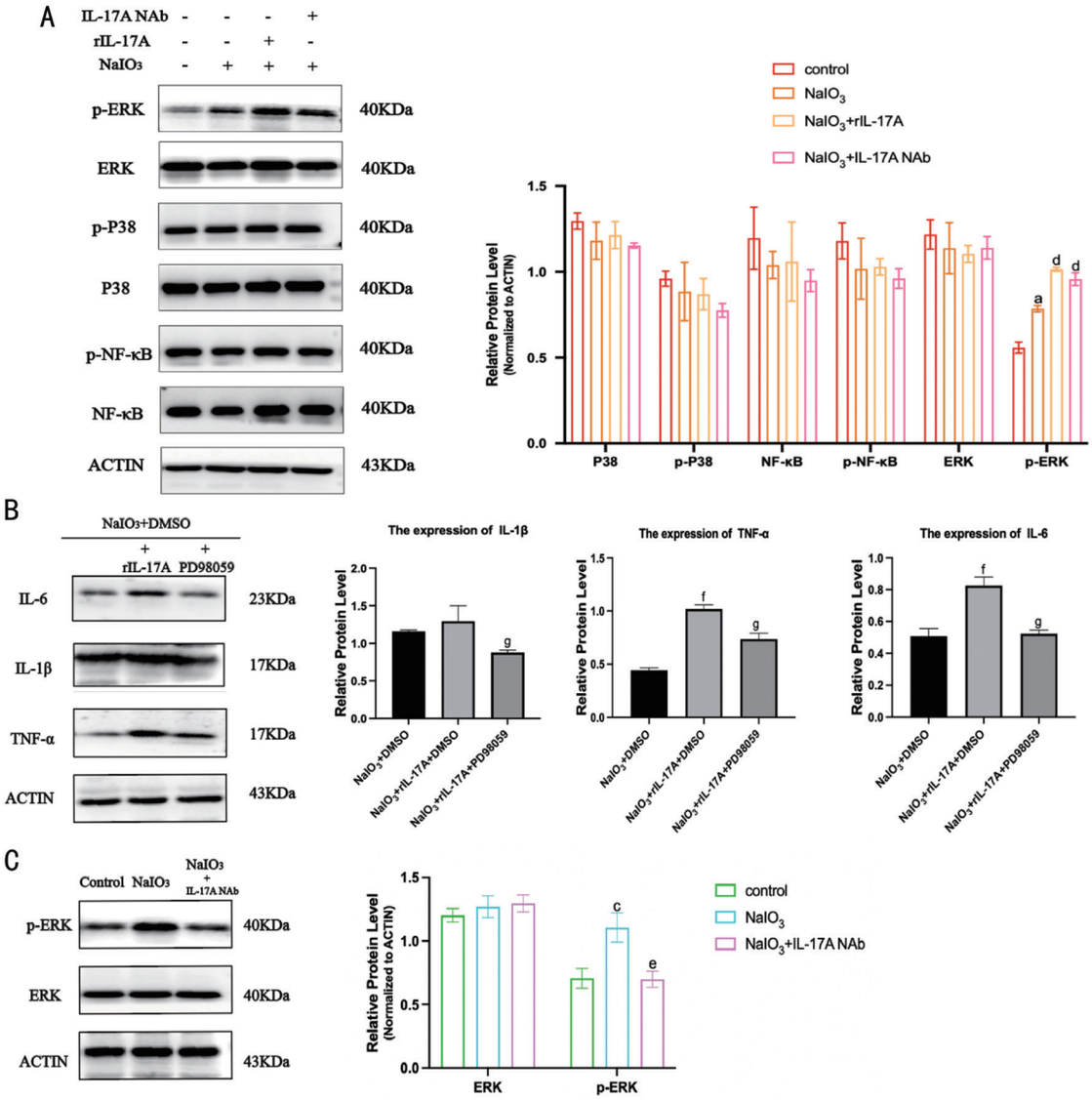

Figure 4 IL-17A regulated proinflammatory cytokines release *via* ERK signaling pathway in $NaIO_3$-induced RPE damage model A: Western blot analysis and grayscale quantification of NF-κB, p-NF-κB, P38, p-P38, ERK, and p-ERK in ARPE-19 cells following $NaIO_3$-induced damage, with or without intervention by rIL-17A or IL-17A Nab; B: Western blot analysis and grayscale quantification of TNF-α, IL-1β, and IL-6 in mice with $NaIO_3$-induced RPE damage, with or without intervention by rIL-17A and PD98059; C: Western blot analysis and grayscale quantification of ERK and p-ERK expression in mouse retina from the control group, $NaIO_3$-only group, and $NaIO_3$+IL-17A NAb group (n=3). Data were represented as mean±SD, ^aP<0.05, ^bP<0.01, ^cP<0.001, and ^dP<0.0001 *vs* control group; ^eP<0.05 *vs* $NaIO_3$ group; ^fP<0.05 *vs* $NaIO_3$+DMSO group; ^gP<0.05 *vs* $NaIO_3$+rIL-17A+DMSO group. $NaIO_3$: Sodium iodate; DMSO: Dimethyl sulfoxide; rIL-17A: Recombinant IL-17A protein; IL-17A Nab: IL-17A neutralizing antibody; RPE: Retinal pigment epithelium; ERK: Extracellular signal-regulated kinase; IL: Interleukin; TNF: Tumor necrosis factor.

the RPE. The expression of p-ERK significantly increased in the $NaIO_3$ model group but was markedly inhibited in the $NaIO_3$+IL-17A NAb treatment group (Figure 4C). These results indicate that the ERK signaling pathway is involved in the regulatory role of IL-17A in $NaIO_3$-induced RPE damage.

IL-17A Knockout Attenuates RPE Degeneration and Microglia Activation in Mice To further investigate whether IL-17A expression affects $NaIO_3$-induced RPE degeneration and microglial activation *in vivo*, morphological and phenotypic examinations were performed on IL-17A$^{-/-}$ mice following intraperitoneal injection of $NaIO_3$. In wild-type mice, microglia were notably activated 5d after $NaIO_3$ injection, and RPE damage was evident in OCT and fundus images. However, in $NaIO_3$-treated IL-17A$^{-/-}$ mice, RPE destruction was mitigated, and microglial activation was reduced, with their morphology remained not fully activated (Figure 5).

DICUSSION

In this study, we reported for the first time that RPE cells can also express IL-17A in situ tissue and in isolated form *in vitro*. Our findings demonstrated that IL-17A may promote the secretion of proinflammatory factors by activating retinal microglia in $NaIO_3$-induced RPE injury model simulating AMD pathology and revealed the protective effect of inhibiting IL-17A on RPE cells.

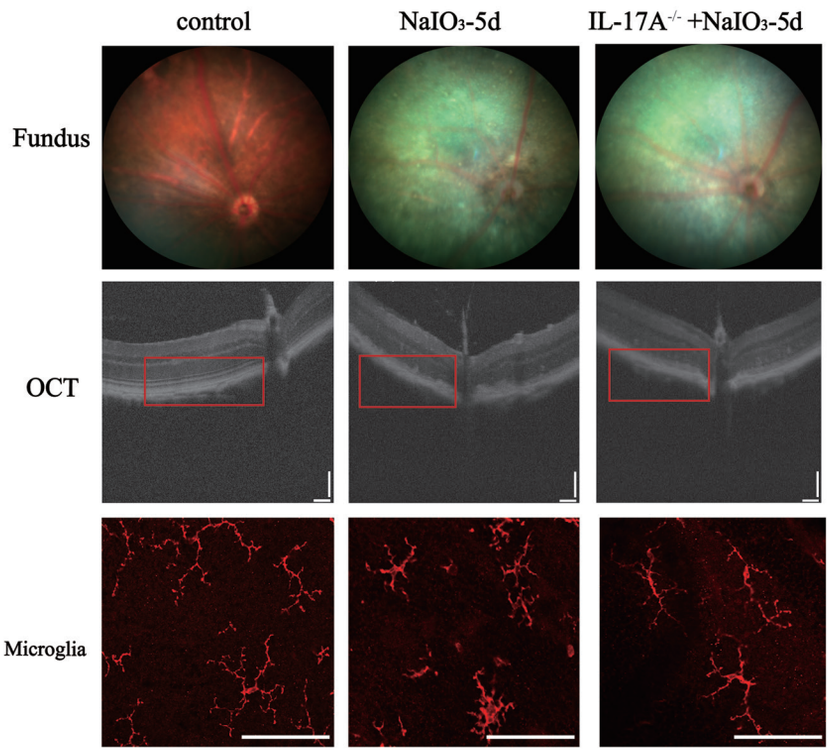

Figure 5 IL-17 knockout can attenuate $NaIO_3$-induced RPE degeneration and microglial activation in mice On day 5 after $NaIO_3$ stimulation, OCT, fundus photography, and IBA-1 immunostaining of retinal whole mounts from wild-type and IL-17A$^{-/-}$ mice were performed (magnification 200×, scale bar = 50 μm). $NaIO_3$: Sodium iodate; RPE: Retinal pigment epithelium; OCT: Optical coherence tomography; IBA-1: Ionized calcium-binding adaptor molecule-1.

For AMD patients, one of the causes of vision loss is the degeneration of RPE cells and photoreceptors[23-24]. The structural changes in retinal damage induced by $NaIO_3$ have been widely reported. Phenotypically, $NaIO_3$-induced retinal damage is similar to non-exudative AMD, including similar fundus and OCT changes[25-27]. Histopathologically, $NaIO_3$-induced RPE atrophy is similar to the pathology of AMD, characterized by distinctive changes in RPE[28]. These findings strongly support that the $NaIO_3$-induced RPE and retinal degeneration model is a suitable animal model for studying non-exudative AMD. Our study also found that after $NaIO_3$ administration, RPE cells began to degenerate, melanin particles aggregated, and their morphology was completely destroyed. Subsequently, in H&E staining, extensive damage, deformation, and reduced thickness of the ONL and IS/OS layers were observed. Both *in vivo* and *in vitro* results of this study indicate that as time progresses after $NaIO_3$ modeling, RPE damage gradually worsens, with a progressive decrease in the expression of the tight junction protein Occludin and an increase in the expression of the oxidative stress-related protein TXNIP.

Although current reports mainly suggest that $NaIO_3$ selectively induces RPE degeneration, our study further found that $NaIO_3$ also leads to the proliferation, migration, and activation of retinal microglia. Retinal microglia are the major cells involved in the immune inflammatory response in retinal degenerative diseases. Retinal microglia migrate and infiltrate into the outer retina under conditions of aging and disease, indicating their involvement in the occurrence and development of AMD[29]. Under normal circumstances, microglia are in a resting state, locating in the inner and outer plexiform layers[30]. When retinal cells are damaged, microglia can rapidly be activated to proliferate and migrate to the damaged site[31-32]. Some researchers have suggested that simply using Western blot to assess the protein expression levels of specific cell markers is insufficient to indicate microglial activation, recommending a multi-faceted evaluation of microglial activation is necessary[33]. Therefore, this study comprehensively assessed the activation status of retinal microglia from the view of both protein expression pattern and morphological changes.

In the pathology of AMD, excessive ROS and oxidized lipoproteins lead to protein misfolding, aggregation, and chronic activation of the innate immune response[34-36]. Oxidative stress and damage are considered key factors triggering RPE degeneration. Oxidative stress ultimately involves excessive ROS which are generated mainly in mitochondria[37]. In this study, we found that the average fluorescence intensity of ROS was enhanced in ARPE-19 cells treated with $NaIO_3$ and rIL-17A together, while IL-17A NAb had the ability to inhibit the excessive production of

intracellular ROS induced by $NaIO_3$. Meanwhile, intracellular NO has various functions in maintaining retinal homeostasis. Under normal physiological conditions, NO synthesis and oxygen radical degradation are in dynamic balance[38]. When this balance is disrupted under pathological conditions, excess free radicals inactivate NO. Clinical studies have shown that NO levels in the plasma of AMD patients are lower[38-39]. Adequate NO concentration is essential for visual management in AMD patients[40]. In the RPE, NO contributes to its phagocytic function and the regulation of *VEGF* gene expression[41-43]. However, the exact role of NO in AMD pathogenesis remains uncertain and requires further exploration. Our study indicates that $NaIO_3$ stimulation leads to the excessive generation of ROS in the RPE cells, and this overly generated trend of ROS was further exacerbated by rIL-17A treatment, whereas was suppressed by IL-17A NAb treatment. The NO levels secreted in the supernatant demonstrated a trend opposite to how ROS level changed under the same treatment respectively. The above results suggested that inhibiting IL-17A can reduce $NaIO_3$-induced oxidative stress in RPE cells.

The inflammatory factors IL-17A, IL-1β, TNF-α and IL-6 are all involved in the irreversible damage to RPE cells. The secretion of the inflammatory factor IL-17A *in vitro* ARPE-19 cell line was detected, showing an initial increase followed by a later decrease, which may be due to increased secretion of IL-17A at an early stage after exogenous stimulation, and then a decrease in secretion due to overwhelming cell damage and impaired cells survival. In the $NaIO_3$-induced RPE damage model, fundus photography and OCT images showed that rIL-17A aggravated RPE detachment and disarray, while neutralizing IL-17A and using IL-17A$^{-/-}$ mice could partially alleviate such RPE damages. Similarly, the trend of inflammatory factors releases in RPE as well as the proliferation and activation of retinal microglia corresponded to the above phenotypes variation. These findings confirmed the accelerator role of IL-17A in the inflammation-related injury process in RPE cells degenerative pathology.

The excessive activation of microglia can lead to neuronal damage through release of a range of toxic substances. Its dual role in the pathophysiological process makes it a "double-edged sword"[31,44]. Chen *et al*[45] found that choroidal γδT cells produce IL-17, which activates RPE cells to produce IL-6, thereby initiating a protective signaling cascade involving mTOR pathway in subretinal microglia. Interestingly, our study found opposite results, where RPE cells can also express IL-17A factor, activating retinal microglia and releasing inflammatory factors, to exacerbate RPE cells injury under degenerative scenario. This finding discovery is consistent with the findings by other researchers that IL-17 exerts pro-inflammatory effects by targeting RPE cells and promoting the evolvement of an inflammatory microenvironment in the eye[46].

Our study further indicated that the ERK signaling pathway is participated in the impact by IL-17A in $NaIO_3$-induced RPE damage. ERK1 and ERK2 are downstream components of the phosphorylation pathway, acting as central regulators of a variety of cellular processes due to their extensive substrate pool. Over the past three decades, the regulatory mechanisms and functions of ERK1 and ERK2, along with their impact on development and homeostasis in different organisms, have been a major focus of attention. Dysregulation of RAS-ERK signaling is associated with a range of human diseases, including cancer, developmental disorders, neurodegeneration, obesity, and aging[47]. A substantial body of literature reports the close link between IL-17A and the ERK pathway in various diseases, such as IL-17A leading to renal fibrosis through the ERK signaling pathway in kidney inflammation[48]. In certain autoimmune diseases, IL-17A also exerts its effects through ERK[49-50]. Other studies have indicated that ERK1/2 is a prominent signaling pathway in cancer, where its phosphorylation can activate Th17 cells, thus inducing inflammatory diseases[51]. To verify whether the ERK signaling pathway truly plays a role, we inhibited the pathway or neutralized IL-17A in our experiments to observe the changes in related inflammatory factors and ERK pathway activity. The results showed that in the context of $NaIO_3$-induced RPE damage in mice, blocking of the ERK signaling pathway resulted in a corresponding decrease in the expression of inflammatory factors like TNF-α, IL-1β, and IL-6, whereas neutralization of IL-17A significantly reduced the activity of ERK pathway, indicating that IL-17A may exerts its proinflammatory effects through the ERK signaling pathway in $NaIO_3$-induced RPE cells injury.

The limitations of this study include the lack of experiments on the migration and phagocytosis characteristics of RPE cells, neither on the interaction between RPE cells and microglia in the current scenario. Additionally, using the ARPE-19 cell line to indirectly study the function/phenotype of RPE *in vivo* has certain limitations. As isolated in the culture environment, the biological behavior of the cell line must change compared to the original RPE cells in situ retina *in vivo* due to the lack of blood supply, neurohumoral regulation, interactions with other cell types and extracellular matrix. Future work plans include exploring the interactions between RPE and microglia, which are crucial for comprehensive understanding of the onset and progression of $NaIO_3$-induced damage and AMD, and further investigating the intrinsic mechanisms behind the observed phenomena.

In conclusion, our data suggest that IL-17A probably promotes the inflammatory response of cytokines release and retinal

microglia activation through the ERK signaling pathway, thereby contributing to the pathogenesis of RPE cells injury. Our study demonstrates the beneficial effects of inhibiting IL-17A in the context of $NaIO_3$-induced RPE cells injury model simulating dry AMD. This provides a theoretical basis for exploration of new promising strategies for the treatment of AMD.

ACKNOWLEDGEMENTS

The authors would like to thank Shou-Yue Huang for the support he provided to this study.

Authors' contributions: Zhong HM and Shen BQ designed and conceived the study. Zhong HM performed the experiments, data collection, data analysis, and article writing. Shen BQ performed the experiments, data collection, and data analysis. Chen YH, Zhao XH, and Huang XX, performed the experiments. Zhou MW and Sun XD revised the manuscript and supervised the whole project.

Foundations: Supported by the National Natural Science Foundation of China (No.82171076; No.U22A20311; No.82388101); the National Key R&D Program (No.2022YFC2502800); Shanghai Municipal Education Commission (No.2023KJ05-67).

Availability of Data and Materials The datasets used and analyzed during the current study are available from the corresponding author on reasonable request.

Conflicts of Interest: Zhong HM, None; **Shen BQ,** None; **Chen YH,** None; **Zhao XH,** None; **Huang XX,** None; **Zhou MW,** None; **Sun XD,** None.

REFERENCES

1 Deng YH, Qiao LF, Du MY, Qu C, Wan L, Li J, Huang LL. Age-related macular degeneration: epidemiology, genetics, pathophysiology, diagnosis, and targeted therapy. *Genes Dis* 2022;9(1):62-79.

2 Wheeler S, Mahmoudzadeh R, Randolph J. Treatment for dry age-related macular degeneration: where we stand in 2024. *Curr Opin Ophthalmol* 2024;35(5):359-364.

3 Wooff Y, Cioanca AV, Wills E, Chu-Tan JA, Sekar R, Natoli R. Short exposure to photo-oxidative damage triggers molecular signals indicative of early retinal degeneration. *Front Immunol* 2023;14:1088654.

4 Bird A. Role of retinal pigment epithelium in age-related macular disease: a systematic review. *Br J Ophthalmol* 2021;105(11):1469-1474.

5 Kushwah N, Bora K, Maurya M, Pavlovich MC, Chen J. Oxidative stress and antioxidants in age-related macular degeneration. *Antioxidants (Basel)* 2023;12(7):1379.

6 Boyer DS, Schmidt-Erfurth U, van Lookeren Campagne M, Henry EC, Brittain C. The pathophysiology of geographic atrophy secondary to age-related macular degeneration and the complement pathway as a therapeutic target. *Retina* 2017;37(5):819-835.

7 Buonfiglio F, Korb CA, Stoffelns B, Pfeiffer N, Gericke A. Recent advances in our understanding of age-related macular degeneration: mitochondrial dysfunction, redox signaling, and the complement system. *Aging Dis* 2024.

8 Kuwabara T, Ishikawa F, Kondo M, Kakiuchi T. The role of IL-17 and related cytokines in inflammatory autoimmune diseases. *Mediators Inflamm* 2017;2017:3908061.

9 Paroli M, Caccavale R, Fiorillo MT, Spadea L, Gumina S, Candela V, Paroli MP. The double game played by Th17 cells in infection: host defense and immunopathology. *Pathogens* 2022;11(12):1547.

10 Li JN, Zhao TT, Sun Y. Interleukin-17A in diabetic retinopathy: The crosstalk of inflammation and angiogenesis. *Biochem Pharmacol* 2024;225:116311.

11 Zhang C, Liu XX, Xiao J, Jiang FW, Fa LZ, Jiang H, Zhou L, Su WR, Xu ZP. γδ T cells in autoimmune uveitis pathogenesis: a promising therapeutic target. *Biochem Pharmacol* 2023;213:115629.

12 Karmoker JR, Bounds SE, Cai JY. Aryl hydrocarbon receptor (AhR)-mediated immune responses to degeneration of the retinal pigment epithelium. *Biochim Biophys Acta Mol Basis Dis* 2024;1870(7):167351.

13 Zhong HM, Sun XD. Contribution of interleukin-17A to retinal degenerative diseases. *Front Immunol* 2022;13:847937.

14 Nassar K, Grisanti S, Elfar E, Lüke, Lüke M, Grisanti S. Serum cytokines as biomarkers for age-related macular degeneration. *Graefes Arch Clin Exp Ophthalmol* 2015;253(5):699-704.

15 Ardeljan D, Wang YJ, Park S, *et al*. Interleukin-17 retinotoxicity is prevented by gene transfer of a soluble interleukin-17 receptor acting as a cytokine blocker: implications for age-related macular degeneration. *PLoS One* 2014;9(4):e95900.

16 Chen JJ, Wang WZ, Li QM. Increased Th1/Th17 responses contribute to low-grade inflammation in age-related macular degeneration. *Cell Physiol Biochem* 2017;44(1):357-367.

17 Fu XY, Wu MX, Zhou XY. Protective effects of 4-octyl itaconate against inflammatory response in angiotensin II-induced oxidative stress in human primary retinal pigment epithelium. *Biochem Biophys Res Commun* 2021;557:77-84.

18 Wang ZJ, Huang YH, Chu FX, Liao K, Cui ZK, Chen JS, Tang SB. Integrated Analysis of DNA methylation and transcriptome profile to identify key features of age-related macular degeneration. *Bioengineered* 2021;12(1):7061-7078.

19 Kolbinger F, Huppertz C, Mir A, Padova FD. IL-17A and multiple sclerosis: signaling pathways, producing cells and target cells in the central nervous system. *Curr Drug Targets* 2016;17(16):1882-1893.

20 Arenas YM, López-Gramaje A, Montoliu C, Llansola M, Felipo V. Increased levels and activation of the IL-17 receptor in microglia contribute to enhanced neuroinflammation in cerebellum of hyperammonemic rats. *Biol Res* 2024;57(1):18.

21 Otero AM, Antonson AM. at the crux of maternal immune activation: Viruses, microglia, microbes, and IL-17A. *Immunol Rev* 2022;311(1):205-223.

22 Chen Y, Chu JMT, Liu JX, Duan YJ, Liang ZK, Zou X, Wei M, Xin WJ, Xu T, Wong GTC, Feng X. Double negative T cells promote surgery-induced neuroinflammation, microglial engulfment and cognitive dysfunction *via* the IL-17/CEBPβ/C3 pathway in adult mice. *Brain Behav Immun* 2024;123:965-981.

23 Giannakaki-Zimmermann H, Querques G, Munch IC, *et al*. Atypical retinal pigment epithelial defects with retained photoreceptor layers: a so far disregarded finding in age related macular degeneration. *BMC Ophthalmol* 2017;17(1):67.

24 Zhang Z, Liang FM, Chang J, Shan XQ, Yin ZX, Wang L, Li SJ. Autophagy in dry AMD: a promising therapeutic strategy for retinal pigment epithelial cell damage. *Exp Eye Res* 2024;242:109889.

25 Xiao JH, Yao JY, Jia L, Lin CM, Zacks DN. Protective effect of Met12, a small peptide inhibitor of fas, on the retinal pigment epithelium and photoreceptor after sodium iodate injury. *Invest Ophthalmol Vis Sci* 2017;58(3):1801-1810.

26 Moriguchi M, Nakamura S, Inoue Y, Nishinaka A, Nakamura M, Shimazawa M, Hara H. Irreversible photoreceptors and RPE cells damage by intravenous sodium iodate in mice is related to macrophage accumulation. *Invest Ophthalmol Vis Sci* 2018;59(8):3476-3487.

27 Koh AE, Alsaeedi HA, Rashid MBA, *et al*. Retinal degeneration rat model: a study on the structural and functional changes in the retina following injection of sodium iodate. *J Photochem Photobiol B* 2019;196:111514.

28 Upadhyay M, Bonilha VL. Regulated cell death pathways in the sodium iodate model: Insights and implications for AMD. *Exp Eye Res* 2024;238:109728.

29 Ma WX, Zhao L, Wong WT. Microglia in the outer retina and their relevance to pathogenesis of age-related macular degeneration. *Adv Exp Med Biol* 2012;723:37-42.

30 O'Koren EG, Yu C, Klingeborn M, *et al*. Microglial function is distinct in different anatomical locations during retinal homeostasis and degeneration. *Immunity* 2019;50(3):723-737.e7.

31 Sierra A, Navascués J, Cuadros MA, Calvente R, Martín-Oliva D, Ferrer-Martín RM, Martín-Estebané M, Carrasco MC, Marín-Teva JL. Expression of inducible nitric oxide synthase (iNOS) in microglia of the developing quail retina. *PLoS One* 2014;9(8):e106048.

32 Lu C, Mao XY, Yuan ST. Decoding physiological and pathological roles of innate immune cells in eye diseases: the perspectives from single-cell RNA sequencing. *Front Immunol* 2024;15:1490719.

33 Norden DM, Trojanowski PJ, Villanueva E, Navarro E, Godbout JP. Sequential activation of microglia and astrocyte cytokine expression precedes increased Iba-1 or GFAP immunoreactivity following systemic immune challenge. *Glia* 2016;64(2):300-316.

34 Kaarniranta K, Koskela A, Felszeghy S, Kivinen N, Salminen A, Kauppinen A. Fatty acids and oxidized lipoproteins contribute to autophagy and innate immunity responses upon the degeneration of retinal pigment epithelium and development of age-related macular degeneration. *Biochimie* 2019;159:49-54.

35 Kulbay M, Wu KY, Nirwal GK, Bélanger P, Tran SD. The role of reactive oxygen species in age-related macular degeneration: a comprehensive review of antioxidant therapies. *Biomedicines* 2024;12(7):1579.

36 Pinelli R, Ferrucci M, Biagioni F, Berti C, Bumah VV, Busceti CL, Puglisi-Allegra S, Lazzeri G, Frati A, Fornai F. Autophagy activation promoted by pulses of light and phytochemicals counteracting oxidative stress during age-related macular degeneration. *Antioxidants* 2023;12(6):1183.

37 Blasiak J, Glowacki S, Kauppinen A, Kaarniranta K. Mitochondrial and nuclear DNA damage and repair in age-related macular degeneration. *Int J Mol Sci* 2013;14(2):2996-3010.

38 Totan Y, Koca C, Erdurmuş M, Keskin U, Yiğitoğlu R. Endothelin-1 and nitric oxide levels in exudative age-related macular degeneration. *J Ophthalmic Vis Res* 2015;10(2):151-154.

39 Totan Y, Cekiç O, Borazan M, Uz E, Sögüt S, Akyol O. Plasma malondialdehyde and nitric oxide levels in age related macular degeneration. *Br J Ophthalmol* 2001;85(12):1426-1428.

40 Cantó A, Olivar T, Romero FJ, Miranda M. Nitrosative stress in retinal pathologies: review. *Antioxidants* 2019;8(11):543.

41 Bhutto IA, Baba T, Merges C, McLeod DS, Lutty GA. Low nitric oxide synthases (NOSs) in eyes with age-related macular degeneration (AMD). *Exp Eye Res* 2010;90(1):155-167.

42 Goldstein IM, Ostwald P, Roth S. Nitric oxide: a review of its role in retinal function and disease. *Vision Res* 1996;36(18):2979-2994.

43 Grunwald JE, Hariprasad SM, DuPont J. Effect of aging on foveolar choroidal circulation. *Arch Ophthalmol* 1998;116(2):150-154.

44 Rivera JC, Sitaras N, Noueihed B, *et al*. Microglia and interleukin-1β in ischemic retinopathy elicit microvascular degeneration through neuronal semaphorin-3A. *Arterioscler Thromb Vasc Biol* 2013;33(8):1881-1891.

45 Chen Y, Bounds SE, Ma X, Karmoker JR, Liu Y, Ma JX, Cai JY. Interleukin-17-mediated protective cytokine signaling against degeneration of the retinal pigment epithelium. *Proc Natl Acad Sci U S A* 2023;120(51):e2311647120.

46 Zhong ZY, Su GN, Kijlstra A, Yang PZ. Activation of the interleukin-23/interleukin-17 signalling pathway in autoinflammatory and autoimmune uveitis. *Prog Retin Eye Res* 2021;80:100866.

47 Lavoie H, Gagnon J, Therrien M. ERK signalling: a master regulator of cell behaviour, life and fate. *Nat Rev Mol Cell Biol* 2020;21(10):607-632.

48 Weng CH, Li YJ, Wu HH, Liu SH, Hsu HH, Chen YC, Yang CW, Chu PH, Tian YC. Interleukin-17A induces renal fibrosis through the ERK and Smad signaling pathways. *Biomed Pharmacother* 2020;123:109741.

49 Chen HL, Lo CH, Huang CC, *et al*. Galectin-7 downregulation in lesional keratinocytes contributes to enhanced IL-17A signaling and skin pathology in psoriasis. *J Clin Invest* 2021;131(1):e130740.

50 Ahmed S, Misra DP, Agarwal V. Interleukin-17 pathways in systemic sclerosis-associated fibrosis. *Rheumatol Int* 2019;39(7):1135-1143.

51 Huang XL, Yu PX, Liu MY, Deng YF, Dong YQ, Liu QH, Zhang JT, Wu T. ERK inhibitor JSI287 alleviates imiquimod-induced mice skin lesions by ERK/IL-17 signaling pathway. *Int Immunopharmacol* 2019;66:236-241.